

CONDENSATION IN MICROCHANNELS WITH A POROUS BOUNDARY: ANALYTICAL INVESTIGATION ON HEAT TRANSFER AND MENISCUS SHAPE

Roger R. Riehl

Ph.D. Candidate – Universidade de São Paulo-EESC/Clemson University
Mechanical Engineering Dept. – Clemson, SC 29634 USA.

Jay M. Ochterbeck

Associate Professor – Clemson University
Mechanical Engineering Dept. – Clemson, SC 29634 USA.

Paulo Selegim, Jr.

Assistant Professor – Universidade de São Paulo – EESC – Dept. Engenharia Mecânica
C.P. 359 – 13560-970 – São Carlos, SP, Brasil.

***Abstract.** In two-phase miniature and microchannel flows, the meniscus shape must be considered due to effects that are affected by condensation and/or evaporation and coupled with the transport phenomena in the thin film on the microchannel wall. This investigation presents an analytical model for microchannel condensers with a porous boundary, where the fluid is pumped by capillary forces. Methanol was selected as the working fluid. Very low liquid Reynolds numbers were obtained ($Re \sim 6$), but very high Nusselt numbers ($Nu \sim 90$) could be found due to the channel size (1.5 mm) and the presence of the porous boundary. The meniscus calculation provided consistent results for the vapor interface temperature and pressure, as well as the meniscus curvature. The obtained results show that microchannel condensers with a porous boundary can be used for heat dissipation with reduced heat transfer area and very high heat dissipation capabilities.*

Keywords: Microchannels, Condensation, Meniscus

1. INTRODUCTION

Previous investigations addressing single-phase and two-phase flows in small diameter and microchannel passages have demonstrated tremendous potential for high heat flux systems with increased heat transport capability. The vast majority of these investigations were directed toward single-phase flow and convective boiling in small diameter and microchannel passages. The basic phenomenon of convective condensation in small diameter/microchannel passages has not been fully addressed experimentally or analytically, especially in the case where the convective condensation phenomenon is coupled with a porous boundary. Better understanding of condensing two-phase flows in small diameter/microchannel passages is an enabling-technology for the development of efficient and reliable two-phase thermal management systems employing small diameter and

microchannel passages, especially for electronics cooling, miniature heat exchangers, and capillary pumped loops.

A literature survey directed toward single-phase and two-phase flow heat transfer coefficients was presented by Riehl et al. (1998) and reviewed the available analytical models and experimental data obtained for microchannels. Of these investigations, Tuckeman and Pease (1981) first investigated systems using microchannel heat exchangers and forced single-phase liquid cooling through microchannels for cooling of electronic devices. The technology demonstrated promise for more compact arrangements. A model was proposed by Weisberg and Bau (1992) which could predict the temperature distribution in a microchannel evaporator for water as working fluid and laminar flow.

Few previous experimental and analytical investigations have been performed regarding microchannels condensation. Smirnov and Buz (1995), Buz and Smirnov (1997) and Smirnov et al. (1997) presented an approach for condensation in small channels. This model was able to predict condensation in channels where the gravitational forces do not influence the flow. Also, the model could predict the liquid film thickness along the channel, which is important for analysis of the condensation capability and is an important factor for determining the meniscus shape.

The meniscus problem was studied for fluid flows in small diameters and primarily for capillary flow. During an investigation of an evaporating meniscus on a flat copper plate, Mirzamoghadam and Catton (1988) found that the interline wall superheat, needed to obtain a converged solution from the steady-state integral model, was in agreement with experimental observations of the wall superheat effect on the meniscus shape. Swanson and Herdt (1992) later developed an analytical model to predict the evaporating meniscus shape with interest in capillary wick structures. The model showed that the maximum capillary pressure cannot be used to evaluate the local interfacial mass transfer rate, which is an intermediate boundary condition between the vapor and liquid phases. DasGupta et al. (1993, 1994) found that the use of Young-Laplace equation could be used to determine the interfacial properties of the system and then describe the process of an evaporating meniscus. This equation showed to accurately predict the meniscus slope.

A model for determining the minimum meniscus radius in micro heat pipes was developed by Ma and Peterson (1998). The obtained equations showed that there is an optimum hydraulic radius for the grooves that have a maximum capillary heat transport capability, which directly affects the meniscus shape. Pratt et al. (1998) experimentally investigated the thermocapillary effects on a curved meniscus and observed that capillary instabilities can result from thermocapillary instabilities of the contact line region of the evaporating meniscus within capillary grooves. This may affect the near contact line region of the extended meniscus formed within the capillary pores.

Much information regarding the single-phase and two-phase (boiling) convective flows in microchannels and the meniscus characteristics in capillary structures have been developed. However, few investigations have attempted to address the condensation phenomena in condensing flows in small diameter/microchannels. This paper presents an analytical investigation of microchannel condensation including liquid film distribution and meniscus shape.

2. ANALYTICAL MODELING IN MICROCHANNEL FLOW

It is important to note that the mathematical formulation developed below for both liquid film distribution and meniscus shape in microchannels assumes that capillary forces pump the condensed liquid throughout the channel.

2.1. Liquid Film Distribution Formulation

Figure 1a presents a general microchannel condenser with a porous boundary which was used in the development of this model. For the case of liquid being pumped through a porous structure, the model geometry is shown in Fig. 1b. As the microchannels were taken to be square, by symmetry only the bottom portion of the channel is represented, where G is the mass flow velocity ($\text{kg}/\text{m}^2 \text{ s}$).

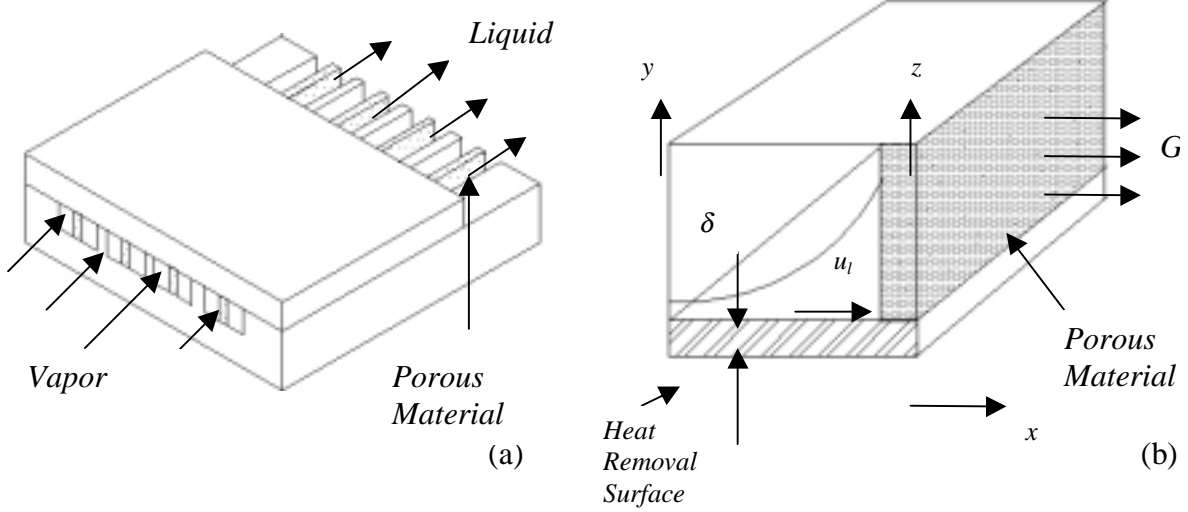


Figure 1 – Flow model for microchannel condensation with a porous wall.

Using the above illustrations and applying the conservation equations of mass, energy and momentum, the resulting derived equation set for the fluid condensing on surfaces x and y , where the porous boundary is not present is given by

$$P' = \frac{dP}{dX} = \text{Re}_l^2 \left(2 \frac{\text{Re}'_l}{\text{Re}_l} + \frac{\Delta'_l}{\Delta_l} \right) + 3 \frac{\text{Re}_l}{\Delta_l^2}, \quad (1)$$

$$\Delta'' = \frac{d^2 \Delta_l}{dX^2} = A \sqrt{1 + \left(\frac{d\Delta_l}{dX} \right)^2} \left[P - \frac{\rho_l}{\rho_v} (\text{Re}'_l \Delta_l + \text{Re}_l \Delta_l')^2 \right], \quad (2)$$

$$\text{Re}'_l = \frac{d \text{Re}_l}{dX} = \frac{H}{\Delta_l^2} - \frac{\text{Re}_l \Delta'_l}{\Delta_l}, \quad (3)$$

$$X = \frac{x}{l}, \quad \Delta = \frac{\delta}{l}, \quad \text{Re}_l = \frac{\rho_l \bar{u}_l l}{\mu_l}, \quad (4)$$

where Re is the Reynolds number, x is the ordinate distance (m), l is the channel length (m), δ is the film thickness (m), ρ is the density (kg/m^3), \bar{u} is the mean velocity (m/s), μ is the viscosity (Pa-s), X is the dimensionless distance and Δ is the dimensionless film thickness. The subscripts l and v represent liquid and vapor phases, respectively. The pumping intensity (P) represents the maximum power that can be obtained by the difference between the liquid and vapor pressure and transport parameters, and is defined as

$$P = \frac{(P_l - P_v)}{v_l^2 \rho_l} l^2, \quad (5)$$

where P is the pressure (Pa) and v is the kinematics viscosity (m^2/s). The dimensionless heat removal (H) is represented as the relation between the heat exchange rate per unit length by the transport properties of the fluid, defined as

$$H = \frac{k_l (T_{sat} - T_w)}{\rho_l v_l i_{lv}}, \quad (6)$$

where k is the thermal conductivity (W/m-K), T_{sat} and T_w are the saturation and wall temperatures (K), respectively, and i_{lv} is the latent heat of vaporization (J/kg). The complex of working fluid (A) represents the maximum heat transport rate per unit of length, as

$$A = \frac{\rho_l v_l^2}{\sigma l} \quad (7)$$

where σ is the fluid surface tension (N/m). For the case of liquid flowing through the porous boundary (z -axis) two other equations were required. These equations are

$$Re' = \frac{d Re_l}{dX} = \frac{Re_l \tan\left(\frac{\beta}{2}\right)}{\Delta_l L^2} - \frac{2 Re_l}{\Delta_l} \frac{d\Delta_l}{dX}, \quad (8)$$

$$P' = \frac{dP_l}{dX} = \frac{J}{8} \frac{[1 + \tan(\beta/2)]^2 Re_l}{\Delta_l^2}, \quad (9)$$

where L is the dimensionless channel length, β is the channel groove angle, and J is an empirical constant used for the solution of flow in porous media and was suggested by Bejan (1991) as equal to 0.55. The boundary conditions used for the solution along the the x and y -axes are

$$\text{at } X = 0 \Rightarrow Re_l = 0; \Delta'_l = 0; P' = 0, \quad (10)$$

$$\text{at } X = 1 \Rightarrow \Delta = \Delta_{X=1}; P = P_{X=1} \quad (11)$$

and for the surface at the z -axis, the boundary conditions are

$$\text{at } X = 0 \Rightarrow Re_{p.m.} = 0, \quad (12)$$

$$\text{at } X = 1 \Rightarrow P = P_{p.m.}; \Delta = \Delta_{p.m.} \quad (13)$$

where the subscript $p.m.$ refers to the porous media. To avoid numerical discontinuity between the y - and x -axes and between x - and z -axes, the following boundary conditions were required

$$\text{at } X = 0 \Rightarrow Re_l = 0; \Delta' = 0, \quad (14)$$

$$\text{at } X = 1 \Rightarrow Re_l = 0; \Delta' = 0 \quad . \quad (15)$$

After solving the system of equations, the Nusselt number can be calculated by

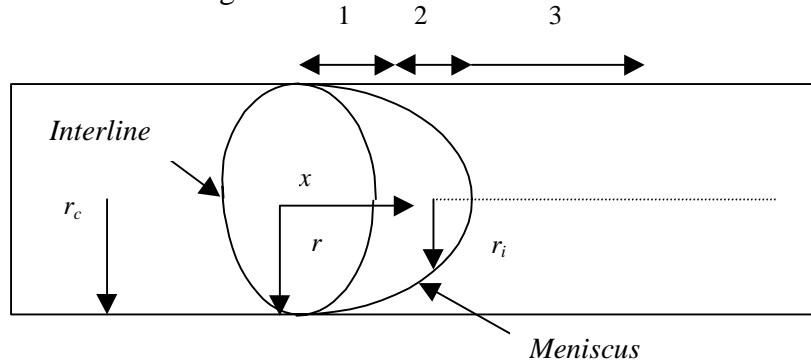
$$Nu = \frac{h_l D_h}{k_l} = \frac{i_{lv} \rho_l \bar{u}_l \delta_l}{k_l (T_{sat} - T_w)} \quad (16)$$

where h is the heat transfer coefficient ($\text{W/m}^2\text{K}$) and D_h is the hydraulics diameter.

2.2. Meniscus Shape Formulation

As the liquid film thickness describes a circular shape in the microchannel, the meniscus shape determination can be conducted using circular coordinates related to the hydraulics diameter. This assumption avoids complicated iterations between the microchannels wall and the liquid film. The meniscus shape formulation describes the fluid mechanics, heat transfer and interfacial phenomena characteristic of a single, isolated condensing meniscus. This formulation includes the three-dimensional Young-Laplace equation, Marangoni convection, London-van der Waals dispersion forces, and non-equilibrium interface conditions. The model used for this formulation is represented by Fig. 2, which shows the transport processes for the meniscus.

In Fig 2, r_c is the hydraulics radius (m), r is the radial coordinate (m) and r_i is the interline radius (m). The model formulation has the following assumptions: 1) channel symmetry, 2) steady state two-dimensional laminar flow, 3) incompressible flow, 4) convective terms, with the exception of the axial convection in the energy equation, are negligible, 5) radial pressure gradient is negligible, 6) temperature in the bulk liquid is equal to the interfacial liquid temperature, 7) pressure in the bulk liquid is constant, 8) no slip at the wall, 9) the channel wall is smooth and the fluid is pure, 10) surface tension (σ) and the dispersion coefficient (\bar{A}) are not affected by the interfacial curvature, 11) retardation effects in the dispersion coefficient are negligible, 12) hydrostatic pressure is negligible and Marangoni effects are important only in the thin-film region.



1 – Thin film region, 2 – Meniscus region; 3 – Hagen-Poiseuille region

Figure 2 – Flow regions for an isolated condensing meniscus in a microchannel.

Using the above assumptions, the system in Fig. 2 and a basic formulation following closely the model of Swanson and Herdt (1992), the equation set that describes the meniscus shape in microchannels condensation is represented as

$$(2\bar{r}_i^2 G_5 - G_3) \frac{d\bar{T}_i}{d\bar{x}} \frac{d\bar{P}_{vi}}{d\bar{x}} + (G_4 - 2\bar{r}_i^2 G_6) D_1 \frac{d\bar{P}_{vi}}{d\bar{x}} + \pi_3 \bar{T}_i - \bar{r}_i G_5 \frac{d\bar{\sigma}}{d\bar{T}_i} \left(\frac{d\bar{T}_i}{d\bar{x}} \right)^2 + \bar{r}_i^2 G_6 \frac{d\bar{\sigma}}{d\bar{T}_i} \frac{d\bar{T}_i}{d\bar{x}} D_1 = 0 \quad (17)$$

$$G_1 \bar{m} \pi_2 - \pi_1 \frac{d\bar{P}_{vi}}{d\bar{x}} + G_2 \frac{d\bar{\sigma}}{d\bar{T}_i} \frac{d\bar{T}_i}{d\bar{x}} = 0, \quad (18)$$

$$\frac{d\bar{m}}{d\bar{x}} + 2\pi\bar{r}_i D_1 \frac{d\bar{T}_i}{d\bar{x}} + \frac{2\pi\bar{r}_i}{1-\bar{r}_i} \bar{T}_i = 0, \quad (19)$$

$$\frac{\pi_4 G_7}{\bar{r}_i} (1+D_1^2)^{3/2} \frac{\cos\theta}{\bar{\sigma}} \frac{d\bar{m}}{d\bar{x}} - \frac{dD_1}{d\bar{x}} + \frac{(1+D_1^2)}{\bar{r}_i} + \frac{(1+D_1^2)^{3/2}}{\bar{\sigma}} \left\{ 4\pi_1 (\bar{P}_{vi} - 1) + \frac{\pi_5}{(1-\bar{r}_i)^3} \right\}, \quad (20)$$

$$\frac{d\bar{r}_i}{d\bar{x}} - D_1 = 0. \quad (21)$$

The set of equations was transformed into dimensionless form by using the following

$$\bar{x} = \frac{x}{r_c}; \quad \bar{r}_i = \frac{r_i}{r_c}; \quad \bar{T}_i = \frac{T_w - T_i}{T_w - T_l}; \quad \bar{K} = Kr_c; \quad \bar{P}_{vi} = \frac{P_{vi}}{P_l}; \quad \bar{m} = \frac{i_{lv}}{r_c k_v (T_w - T_l)} \dot{m}; \quad \bar{\sigma} = \frac{\sigma}{\sigma_w(T_w)},$$

where P_{vi} is the interface vapor pressure (Pa), \bar{P}_{vi} and \bar{T}_i are the dimensionless interface vapor pressure and temperature, T_i is the interface temperature (K), K is the meniscus curvature (m) and \bar{K} is the dimensionless meniscus curvature, \dot{m} and \bar{m} are the liquid mass flow between the interface and tube wall (kg/s) and its dimensionless form. The variables G_1 , G_2 , G_3 , G_4 , G_5 , G_6 and G_7 , are dimensionless functions, defined as

$$G_1 = \frac{1}{2\bar{r}_i^4 - 4\bar{r}_i^2 + 2 - 4(\bar{r}_i^4 - \bar{r}_i^2) \ln \bar{r}_i}, \quad (22)$$

$$G_2 = 4(\bar{r}_i^3 - \bar{r}_i) \ln \bar{r}_i G_1, \quad (23)$$

$$G_3 = -\frac{1}{4}(1-\bar{r}_i^2)^2 - \frac{-\frac{2}{5} + \frac{\bar{r}_i^5}{20} + \frac{\bar{r}_i}{4} - \frac{\bar{r}_i^3}{6}}{1-\bar{r}_i}, \quad (24)$$

$$G_4 = \frac{T_w}{T_w - T_v} (\bar{r}_i - \bar{r}_i^3) - (-\bar{r}_i^3 + \bar{r}_i) \bar{T}_i - \frac{1}{4} \frac{(1-\bar{r}_i^2)^2}{1-\bar{r}_i} \bar{T}_i + \frac{-\frac{2}{5} + \frac{\bar{r}_i^5}{20} + \frac{\bar{r}_i}{4} - \frac{\bar{r}_i^3}{6}}{(1-\bar{r}_i)^2} \bar{T}_i, \quad (25)$$

$$G_5 = -\frac{\bar{r}_i^2}{2} \ln \bar{r}_i - \frac{1-\bar{r}_i^2}{4} - \frac{\frac{\bar{r}_i^3}{6} \ln \bar{r}_i - \frac{\bar{r}_i^3}{9} + \frac{\bar{r}_i}{4} - \frac{5}{36} \bar{r}_i^3}{1-\bar{r}_i}, \quad (26)$$

$$G_6 = -\frac{T_w}{T_w - T_v} \bar{r}_i \ln \bar{r}_i + \bar{r}_i \bar{T}_i \ln \bar{r}_i + \frac{\bar{r}_i^2 \ln \bar{r}_i + \frac{1 - \bar{r}_i^2}{4}}{1 - \bar{r}_i} \bar{T}_i - \frac{\bar{r}_i^3 \ln \bar{r}_i - \frac{1}{9} + \frac{\bar{r}_i}{4} - \frac{5}{36} \bar{r}_i^3}{(1 - \bar{r}_i)^2} \bar{T}_i, \quad (27)$$

$$G_7 = \left(\frac{T_w}{T_w - T_l} - \bar{T}_i \right)^{1/2}. \quad (28)$$

Scaling for this analysis used the variables π_1 , π_2 , π_3 , π_4 and π_5 , which were defined as

$$\pi_1 = \frac{P_v r_c}{4\sigma_p}, \quad \pi_2 = \frac{2\mu_v k_v (T_w - T_l)}{r_c \rho_v \pi_{lv} \sigma_w}, \quad \pi_3 = \frac{\alpha \mu_v}{r_c \sigma_w}, \quad \pi_4 = \left(\frac{2 - C}{2C} \right) \frac{R^{1/2} k_v (T_w - T_l)^{3/2}}{(2\pi)^{1/2} \sigma_w i_{lv}}, \quad \pi_5 = \frac{-\bar{A}}{\sigma_w r_c^2}$$

where C is the accommodation coefficient and R is the gas constant (J/kg K). Physical meaning of the dimensionless variables can be expressed as: π_1 is the dimensionless pumping resistance, π_2 is the dimensionless subcooling; π_3 is the Crispation number; π_4 is the mass flux at the interface and π_5 is the dispersion number, which denotes the magnitude of the dispersion forces in the thin film.

3. SOLUTION METHOD FOR THE PROPOSED MODEL

The solution method used for solving the presented set of equations required constant iteration between both models. First, the equation set derived for solving the liquid film distribution was solved using the Runge-Kutta 4th Order Method. Equations (1)-(3) were solved separately for the x and y -axis and eqs. (2), (8) and (9) were solved for the z -axis (porous boundary) using the boundary conditions (10)-(15). An iterative matching solution has to be applied in order to avoid numerical discontinuities between y and x -axis and between x and z -axis.

For the meniscus shape equation set, the initial values of the dependent variables were selected as

$$\bar{T}_{i,0} = 0.1, \quad \bar{m}_{i,0} = -1E - 11, \quad \bar{r}_{i,0} = 1 - \left(\frac{-\bar{A} T_l}{\rho_v r_c^3 i_{lv} (T_w - T_l)} \right)^{1/3}, \quad \bar{P}_{vi,0} = 1 - \frac{1}{4\pi_i \bar{r}_{i,0}} - \frac{\rho_v i_{lv} (T_w - T_l)}{P_l T_l}.$$

At each value of film thickness resulting from the calculation, the equation set for the meniscus shape, represented by eqs. (17)-(21) was solved using both partial linearization (using Taylor series) and backward finite differentiation. The non-linear terms of eq. (17) were first linearized around the previous iteration. Then, with the transformed form of Eq. (17), the resulting equation set was solved by a backward first-order finite differentiation method. The resulting linear equation set was then solved using a Gauss-Seidel numerical method.

Despite the complexity of the equation solutions, the system provides good convergence. For the liquid film thickness, the equation set calculation presented stable solutions. For the meniscus shape equations, the system converged within three to five iterations for each axial position with a relative error of 10^{-10} and a step size of 10^{-30} . The solution could be reached over the interval $0.115 \leq \bar{r}_i \leq 1.0$. For $\bar{r}_i > 0.115$ the equation set became unstable and D_l approaches negative infinity. At this point, the meniscus shape presents almost no change and

the results could be neglected as it approaches Hagen-Poiseuille flow. Using a Pentium II 300 MHz computer, the overall solution time was less than five minutes.

4. RESULTS AND DISCUSSION

The proposed model was calculated for a microchannel condenser with channel size of $D_h=1.5\text{ mm}$, $\delta = 0.01\text{ mm}$, vapor pressure of 30 kPa, and methanol as the working fluid. It was assumed that $T_{sat}=55\text{ }^\circ\text{C}$, $\bar{u}_l=3\text{ mm/s}$, $L=150\text{ mm}$, and $\beta=0$. The thermophysical properties used in this solution were obtained from Peterson (1994). Figures 3a, 3b and 3c show the liquid film distribution along the x -, y - and z -axes, respectively, and Fig. 3d presents the Nusselt number.

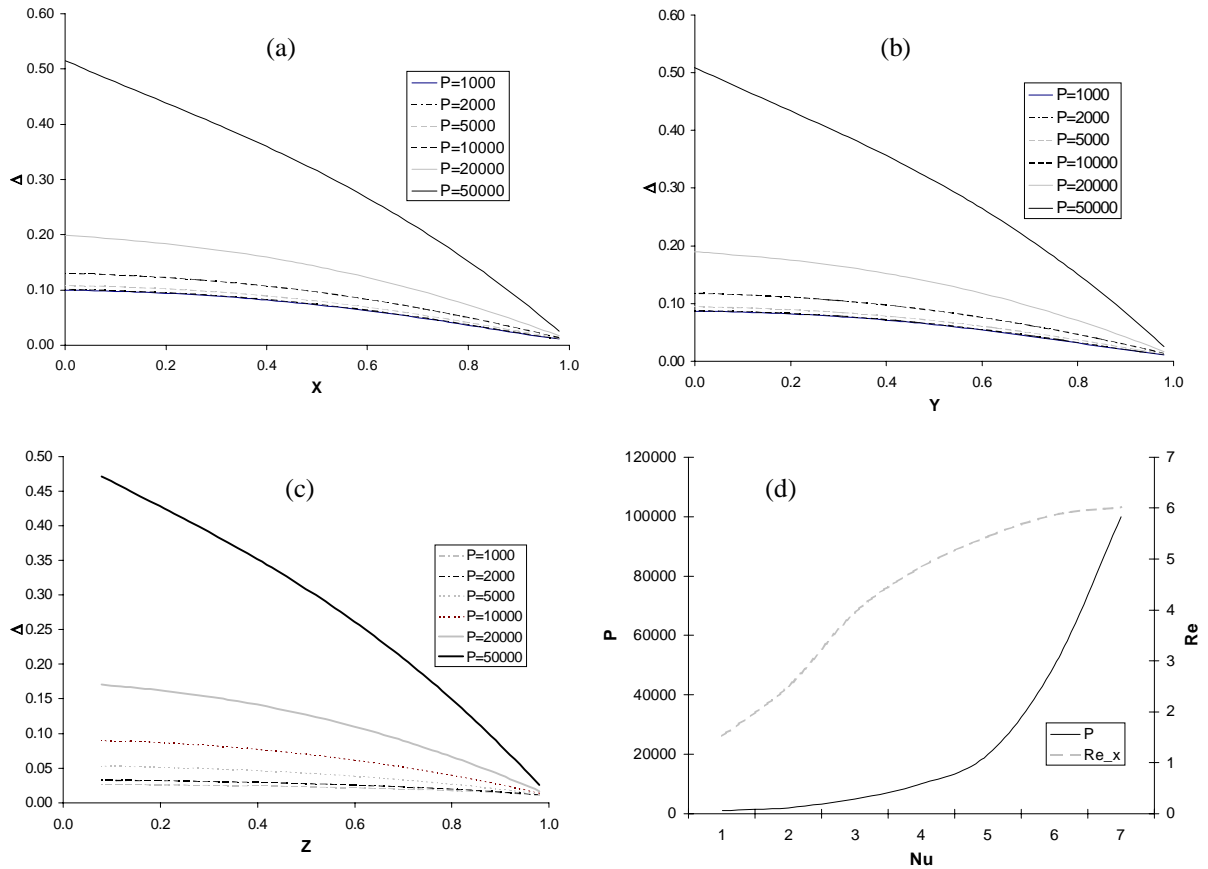


Figure 3 – Liquid film distributions and Nusselt number.

The results presented by the graphs show that when the liquid has been removed for high values of pumping intensity, the condensing film is characterized by a considerable and non-monotonous change of pressure gradient P' along the liquid film. The insignificant influence of inertial forces on Nusselt number is observed. Also, the dependence of the average intensity of heat exchange on the pumping intensity testifies that there is a maximum for heat removal. When this maximum is reached, even for a higher pumping intensity, the heat exchange rate will not increase. The dependence of the Nusselt number with the pumping intensity and the Reynolds number is clear in the results, where Nusselt number increases for higher pumping intensities and Reynolds number. Figures 4 and 5 show the results for the condensing meniscus in the case of a film thickness of 0.01 mm.

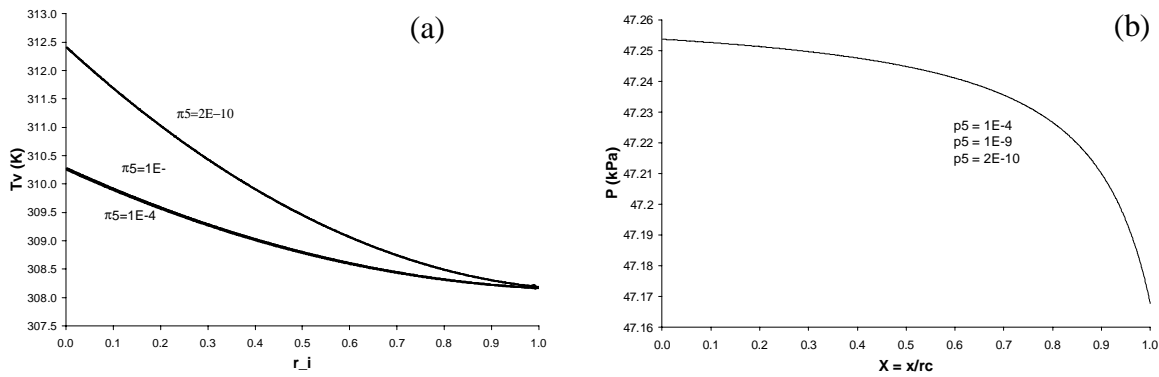


Figure 4 – Vapor temperature and pressure at the interface for a condensing meniscus.

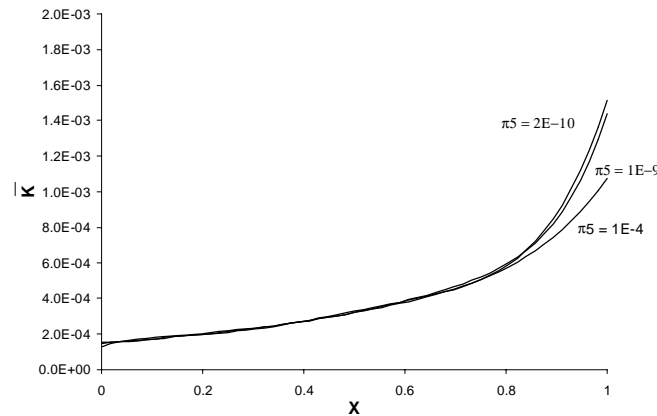


Figure 5 – Dimensionless mean curvature profile for a condensing meniscus.

Figure 4a shows that the dispersion number (π_5) represents a large influence on the vapor temperature at the interface. For a dispersion number of 2×10^{-10} , the dispersion forces in the thin film present a strong influence and result in a temperature difference between the center of the channel and the wall of around 4.5 K. Although a great difference is not observed for dispersion numbers of 1×10^{-4} and 1×10^{-9} . On a microscopic level, the characteristic of the menisci is that for larger dispersion numbers, the thin film extends further down along the channel due to the attractive forces between the vapor and the solid substrate. Such attraction forces can be observed in Fig. 4b. The same results were obtained for different dispersion numbers, which means that the vapor pressure at the interface is not affected by this parameter. Although, as the vapor interface approaches the wall, there is a pressure drop due to the attraction forces. Figure 5 presents the dimensionless meniscus curvature, which is influenced highly by the dispersion number by the same reasons explained above.

The current model has been proposed as a tool to aid in the design of microchannel condensers with possible applications to microelectronics cooling, micro heat exchangers, and condensers in capillary pumped loops and loop heat pipes with restricted heat dissipation area. Validation of the model with experimental investigation is required and planned for the near future.

Acknowledgements

Mr. R. Riehl wishes to thank the scholarship support from the Fulbright Foundation, CAPES (Brazil), and the University of Sao Paulo-EESC (Brazil).

5. REFERENCES

- Bejan, A., 1995, Convection heat transfer. 2nd Edition, John Wiley and Sons.
- Buz, V. N., H. F. Smirnov, H. F., 1997, The film-wise condensation on the finned surfaces and with artificial suction in space conditions. The general analysis, modeling, research. Proceedings of the Physics of Heat Transfer in Boiling and Condensation, May 21-24, Moscow, pp. 545-549.
- DasGupta, S., Schonberg, J. A., Wayner Jr., P. C., 1993, Investigation of an evaporating extended meniscus based on the augmented Young-Laplace equation. ASME Journal of Heat Transfer, Vol. 115, pp. 201-208.
- DasGupta, S., Kim, I., Y., Wayner Jr., P. C., 1994, Use of the Kelvin-Clayperon equation to model an evaporating curved microfilm, ASME Journal of Heat Transfer, Vol. 116, pp. 1007-1014.
- Ma, H.B., Peterson, G. P., 1998, The minimum meniscus radius and capillary heat transport limit in micro heat pipes, ASME Journal of Heat Transfer, Vol. 120, pp. 227-233.
- Mirzamoghadam, A., Catton, I., 1988, A physical model of the evaporating meniscus. ASME Journal of Heat Transfer, Vol. 110, pp. 201-207.
- Peterson, G. P., 1994, An Introduction to Heat Pipes, John Wiley & Sons, New York.
- Pratt, D. M., Brown, J. R., Hallinan, K. P., 1998, Thermocapillary effects on the stability of a heated curved meniscus, ASME Journal of Heat Transfer, Vol. 120, pp. 220-226.
- Riehl, R. R.; Seleglim Jr., P.; Ochterbeck, J. M., 1998, Comparison of heat transfer correlations for single- and two-phase microchannel flows for microelectronics cooling. ITherm'98 Conference, Seattle – Washington May 27-30, pp. 409-416.
- Smirnov, H. F., Buz, V. N., 1995, The condensation on the finned, corrugated surfaces when the condensate film flows without gravitational forces action. Proceedings of the IX International Heat Pipe Conference, May 1-5, Albuquerque-NM, Vol.1, pp.509-513.
- Smirnov, H. F., Buz, V. N., Goncharov, K. A., 1997, Intensification of heat exchange in two-phase loop condensers of space application. Proceedings of the 10th International Heat Pipe Conference, September 21-25, Stuttgart, pp. 1-11.
- Swanson, L. S., Herdt, G. C., 1992, Model of the evaporating meniscus in a capillary tube. ASME Journal of Heat Transfer, Vol. 114, pp. 434-441.
- Tuckermann, D. B.; Pease, R. F. W., 1981, High-performance heat sinking for VLSI. IEEE Electron Device Letters, Vol. EDL-2, No.5, pp. 126-129.
- Weisberg, A.; Bau, H. H., 1992, Analysis of microchannels for integrated cooling. Int. J. Heat Mass Transfer, Vol. 35, No. 10, pp. 2465-2474.